

Probes of Diffusive Shock Acceleration using Gamma-Ray Burst Prompt Emission

Matthew G. Baring

Department of Physics and Astronomy, MS-108, Rice University, P. O. Box 1892,
Houston, TX 77251-1892, USA Email: baring@rice.edu

Abstract. The principal paradigm for gamma-ray bursts (GRBs) suggests that the prompt transient gamma-ray signal arises from multiple shocks internal to the relativistic expansion. This paper explores how GRB prompt emission spectra can constrain electron (or ion) acceleration properties at the relativistic shocks that pertain to GRB models. The array of possible high-energy power-law indices in accelerated populations is highlighted, focusing on how spectra above 1 MeV can probe the field obliquity in GRB internal shocks, and the character of hydromagnetic turbulence in their environs. When encompassing the MeV-band spectral break, fits to BATSE/EGRET burst data indicate that the preponderance of electrons responsible for the prompt emission reside in an intrinsically non-thermal population. This differs markedly from typical populations generated in acceleration simulations; potential resolutions of this conflict such as the action of self-absorption are mentioned. Spectral modeling also suggests that the synchrotron mechanism is favored over synchrotron self-Compton scenarios due to the latter's typically broad curvature near the peak. Such diagnostics will be enhanced by the broadband spectral coverage of bursts by the *Fermi* Gamma-Ray Space Telescope; the GBM will provide key information on the lower energy portions of the non-thermal particle population, while the LAT will constrain the power-law regime of particle acceleration.

Keywords: Gamma-ray bursts, non-thermal emission; diffusive shock acceleration; hydromagnetic turbulence

PACS: 98.70.Rz; 95.85.Pw; 98.70.Sa; 52.35.Ra; 52.25.Xz; 52.27.Ny; 52.35.Tc; 52.65.Pp

INTRODUCTION

The gamma-ray burst paradigm has evolved dramatically over the last decade since the first redshift determinations provided unambiguous evidence for a cosmological distance scale. Yet much is still to be learned about associations, progenitors, and the environment of both the prompt and afterglow emission regions, and the physical processes active therein. For prompt burst emission, the measurement of the high energy spectral index provides a key constraint on the interpretation of the electron acceleration process. Presuming the popular burst paradigm of radiative dissipation at internal shocks that accelerate particles [1–3], it is of great interest to understand what physical conditions in the shocked environs can elicit the observed indices and the spectral structure around the MeV-band peak. To assess this, one turns to models of diffusive shock acceleration in relativistic systems. These come in different varieties, including semi-analytic solutions of the diffusion-convection equation [4, 5], Monte Carlo simulations [6–9], and particle-in-cell (PIC) full plasma simulations [10–13]. Each has its merits and limitations. Tractability of the analytic approaches generally restricts solution to power-law regimes for the particle momentum distributions. PIC codes are rich in their information on turbulence and shock-layer electrodynamics. To interface with GRB data, a broad dynamic range in momenta is desirable, and this is the natural niche of Monte Carlo simulation techniques, the focus of this paper.

A key property of acceleration at the relativistic shocks that are presumed to seed prompt GRB radiative dissipation is that the distribution functions $f(\mathbf{p})$ are inherently anisotropic. This renders the power-law indices and other distribution characteristics sensitive to directional influences such as the magnetic field orientation, and the nature of MHD turbulence that often propagates along the field lines. Accordingly, familiar results from relativistic shock acceleration theory such as the so-called canonical $\sigma = 2.23$ power-law index [5], while providing useful insights, are of fairly limited applicability. This is fortunate since the GRB database so far has exhibited a substantial range of spectral characteristics, so any universal signature in the acceleration predictions would be unnecessarily limiting. This paper explores some of the features of diffusive shock acceleration using results from a Monte Carlo simulation, and addresses probes of the theoretical parameter space imposed by extant GRB observations around and above the MeV spectral break. Palpable diagnostics [14] have already been enabled by data provided by the BATSE and EGRET instruments on the Compton Gamma-Ray Observatory (CGRO) for a handful of bright bursts. The burst community expects significant advances in the understanding of such constraints in the next few years, afforded by the broad spectral coverage and sensitivity of the GBM and LAT experiments on NASA's *Fermi* Gamma-Ray Space Telescope.

DIFFUSIVE ACCELERATION AT RELATIVISTIC SHOCKS

Most internal GRB shocks that are putatively responsible for the prompt emission are mildly-relativistic because they are formed by the collision of two ultra-relativistic shells. Hence, this regime forms the focus of this exposition. The discussion will address the theoretical methodology employed, and the resulting characteristics of the diffusive acceleration process, before moving onto constraints on theoretical parameters imposed by the prompt GRB observations.

The simulation used here to calculate diffusive acceleration in relativistic planar shocks is a kinematic Monte Carlo technique that has been employed extensively in supernova remnant and heliospheric contexts, and is described in detail in numerous papers [6, 7, 15–18]. It is conceptually similar to Bell’s [19] test particle approach to diffusive shock acceleration. Particles are injected upstream and gyrate in a laminar electromagnetic field, with their trajectories being governed by a relativistic Lorentz force equation in the frame of the shock. In general, the fluid frame magnetic field is inclined at an angle Θ_{Bf1} to the shock normal. Because the shock is moving with a velocity $\mathbf{u}(\mathbf{x})$ relative to the plasma rest frame, there is, in general, a $\mathbf{u} \times \mathbf{B}$ electric field in addition to the bulk magnetic field. Particle interactions with Alfvén wave and other hydromagnetic turbulence is modeled by using a phenomenological scattering of the charges in the rest frame of the plasma. The scattering precipitates spatial diffusion of particles along magnetic field lines, and to a varying extent, across them as well. The scatterings are also assumed to be quasi-elastic, an idealization that is usually valid because in most astrophysical systems the flow speed far exceeds the Alfvén speed, and contributions from stochastic second-order Fermi acceleration are small. The diffusion permits a minority of particles to transit the shock plane numerous times, gaining energy with each crossing via the shock drift and first-order Fermi processes.

A continuum of scattering angles, between large-angle (LAS) or small-angle cases, can be modeled by the simulation. In the local fluid frame, the time, δt_f , between scatterings is coupled [6] to the mean free path, λ , and the maximum scattering (i.e. momentum deflection) angle, θ_{scatt} via $\delta t_f \approx \lambda \theta_{\text{scatt}}^2 / (6v)$ for particles of speed $v \approx c$. Usually λ is assumed to be proportional to a power of the particle momentum p (see [6, 20] for microphysical justifications for this choice), and for simplicity it is presumed to scale as the particle gyroradius, r_g , i.e. $\lambda = \eta r_g \propto p$. The parameter η in the model is a measure of the level of turbulence present in the system, coupling directly to the amount of cross-field diffusion, such that $\eta = 1$ corresponds to the isotropic *Bohm diffusion* limit, where the field fluctuations satisfy $\delta B/B \sim 1$. In kinetic theory, η couples the parallel ($\kappa_{\parallel} = \lambda v/3$) and perpendicular (κ_{\perp}) spatial diffusion coefficients via the relation $\kappa_{\perp}/\kappa_{\parallel} = 1/(1 + \eta^2)$ [16, 21]. In parallel shocks, where the \mathbf{B} field is directed along the shock normal ($\Theta_{\text{Bf1}} = 0$), η has only limited impact on the resulting energy spectrum, principally determining the diffusive spatial scale normal to the shock. However, in oblique relativistic shocks where $\Theta_{\text{Bf1}} > 0$, the diffusive transport of particles across the field (and hence across the shock) becomes critical to retention of them in the acceleration process. Accordingly, for such systems, the interplay between the field angle and the value of η controls the spectral index of the particle distribution [7, 22], a feature that is central to the interpretation of GRB spectra below.

Acceleration Properties at Relativistic Shocks

Representative particle differential distributions dN/dp that result from the simulation of diffusive acceleration at mildly-relativistic (internal GRB) shocks are depicted in the *left panel* of Figure 1 (see [7, 9] for $\Gamma_1 \gg 1$ simulation results); these distributions are equally applicable to electrons or ions, and so the mass scale is not specified. A striking feature is that the slope and shape of the non-thermal particle distribution depends on the nature of the scattering. The often cited asymptotic, ultrarelativistic index of $\sigma = 2.23$ for $dN/dp \propto p^{-\sigma}$ is realized only for parallel shocks with $\Theta_{\text{Bf1}} = 0^\circ$ in the mathematical limit of small (pitch) angle diffusion (PAD), where the particle momentum is stochastically deflected on arbitrarily small angular (and therefore temporal) scales. In practice, PAD results when the maximum scattering angle θ_{scatt} is inferior to the Lorentz cone angle $1/\Gamma_1$ in the upstream region. In such cases, particles diffuse in the region upstream of the shock only until their velocity’s angle to the shock normal exceeds around $1/\Gamma_1$, after which they are rapidly swept downstream of the shock. The Figure indicates clearly that when the field obliquity increases, so also does the index σ , with values greater than $\sigma \sim 3$ arising for $\Theta_{\text{Bf1}} \gtrsim 50^\circ$ for this mildly-relativistic scenario. This is a consequence of more prolific convection downstream away from the shock.

Figure 1 also shows results for large angle scattering scenarios (LAS, with $4/\Gamma_1 \lesssim \theta_{\text{scatt}} \lesssim \pi$), where the distribution is highly structured and much flatter on average than p^{-2} . The structure becomes more pronounced for large Γ_1 [7, 9, 22], and is kinematic in origin, where large angle deflections lead to fractional energy gains between unity and Γ_1^2 in successive shock crossings. Each structured bump or spectral segment corresponds to an increment of two in the number of shock transits. For $p \gg mc$, they asymptotically relax to a power-law, in this case with index $\sigma \approx 1.62$.

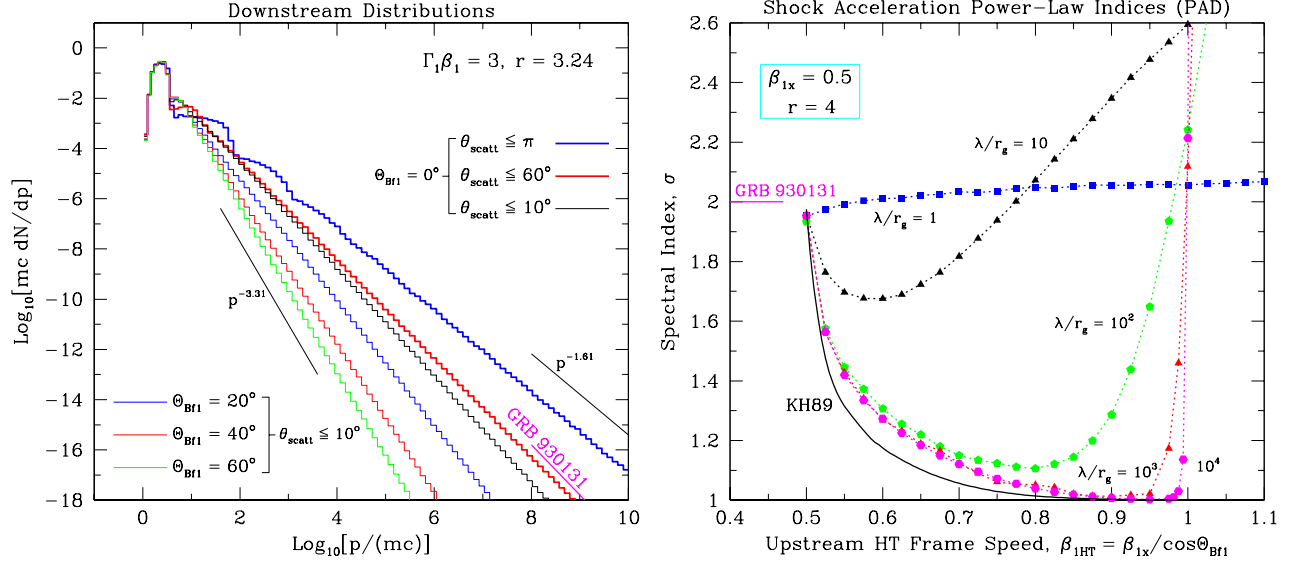


FIGURE 1. *Left panel:* Particle distribution functions dN/dp from mildly-relativistic shocks ($\Gamma_1\beta_1 = 3$, i.e. $\beta_1 = u_1/c = 0.949$) of upstream-to-downstream velocity compression ratio $r = u_{1x}/u_{2x} \approx 3.24$. Simulation results can be divided into two groups: parallel shock runs ($\Theta_{\text{Bf1}} = 0^\circ$, upper three histograms), and oblique, superluminal shock cases ($\Theta_{\text{Bf1}} = 20^\circ, 40^\circ, 60^\circ$, lower three histograms). Scattering off hydromagnetic turbulence was modeled by randomly deflecting particle momenta by an angle within a cone, of half-angle θ_{scatt} , whose axis coincides with the particle momentum prior to scattering; the ratio of the diffusive mean free path λ to the gyroradius r_g was fixed at $\eta = \lambda/r_g = 5$. The heavyweight lines (two uppermost histograms) are for the large angle scattering cases (LAS: $1/\Gamma_1 \ll \theta_{\text{scatt}} \leq \pi$). All other cases constitute pitch angle diffusion (PAD) runs, when $\theta_{\text{scatt}} \lesssim 1/\Gamma_1$ and the distributions become independent of the choice of θ_{scatt} . All distributions asymptotically approach power-laws $dN/dp \propto p^{-\sigma}$ at high energies. For the two cases bracketing the results depicted, the power-laws are indicated by lightweight lines, with indices of $\sigma = 1.61$ ($\Theta_{\text{Bf1}} = 0^\circ$, $\theta_{\text{scatt}} \leq \pi$) and $\sigma = 3.31$ ($\Theta_{\text{Bf1}} = 60^\circ$, $\theta_{\text{scatt}} \leq 10^\circ$), respectively. *Right panel:* Power-law indices σ for simulation runs in the limit of small angle scattering (pitch angle diffusion), for an almost non-relativistic shock of upstream flow speed $\beta_{1x} \equiv u_{1x}/c = 0.5$, and an MHD velocity compression ratio $r = 4$. The indices are displayed as functions of the effective de Hoffman-Teller frame upstream flow speed $\beta_{1\text{HT}} = \beta_{1x}/\cos\Theta_{\text{Bf1}}$, with select values of the fluid frame field obliquity Θ_{Bf1} marked at the top of the panel. Obliquities for which $\beta_{1\text{HT}} > 1$ constitute superluminal shocks. The displayed simulation index results were obtained for different diffusive mean free paths λ parallel to the mean field direction, namely $\lambda/r_g = 1$ (blue squares), $\lambda/r_g = 10$ (black triangles), $\lambda/r_g = 10^2$ (green pentagons), $\lambda/r_g = 10^3$ (red triangles) and $\lambda/r_g = 10^4$ (magenta hexagons), as labelled. The lightweight black curve at the bottom labelled KH89 defines the semi-analytic result from Kirk & Heavens' [4] solution to the diffusion-convection equation, corresponding to $\lambda/r_g \rightarrow \infty$. *Both panels:* The short heavyweight magenta lines labelled GRB 930131 indicate the approximate spectral index σ that is appropriate for this EGRET burst, if a cooled synchrotron emission scenario is operable (see text for a discussion).

Intermediate cases are also depicted in Figure 1, with $\theta_{\text{scatt}} \sim 4/\Gamma_1$. The spectrum is smooth, like for the PAD case, but the index is lower than 2.23. From the plasma physics perspective, magnetic turbulence could easily be sufficient to effect scatterings on this intermediate angular scale, a contention that becomes even more germane for ultrarelativistic shocks [9]. Astrophysically, such flat distributions may prove desirable in models of GRB or blazar jet emission, particularly if efficient radiative cooling is invoked. Note that acceleration distributions are qualitatively similar for ultra-relativistic shocks, i.e. those perhaps more appropriate for GRB afterglow studies, with a trend [5–7, 9, 22] of declining σ for higher Γ_1 , the consequence of an increased kinematic energy boosting in collisions with turbulence.

It is clear that there is a considerable range of indices σ possible for non-thermal particles accelerated in mildly relativistic shocks, a non-universality that can attractively mesh with GRB observations. The two key parameters that dictate the array of possible spectral indices σ are the shock field obliquity Θ_{Bf1} , and the ratio $\eta = \lambda/r_g$ of the diffusive mean free path to the particle's gyroradius r_g . A parameter survey for diffusive acceleration at a typical mildly-relativistic shock is exhibited in the *right panel* of Fig. 1, where only the pitch angle diffusion limit was employed. The power-law index σ is plotted as a function of the de Hoffman-Teller (HT [23]) frame dimensionless speed $\beta_{1\text{HT}} = \beta_{1x}/\cos\Theta_{\text{Bf1}}$, where the subscript x denotes components along the shock normal. This is the upstream flow speed in the shock rest frame where the flow is everywhere parallel to the magnetic field; it corresponds to a

physical speed when $\beta_{\text{1HT}} < 1$ (i.e. the upstream field obliquity satisfies $\cos\Theta_{\text{Bfl}} < \beta_{1x}$, and the shock is said to be *subluminal*. When mathematically $\beta_{\text{1HT}} > 1$, the shock is termed *superluminal*, and the de Hoffman-Teller frame technically does not exist — no Lorentz boost can render the flow parallel to \mathbf{B} . Clearly, the x-axis maps variations in Θ_{Bfl} , with more highly oblique shocks corresponding to the right of the plot.

A feature of this plot is that the dependence of σ on field obliquity is non-monotonic. When $\lambda/r_g \gg 1$, the value of σ at first declines as Θ_{Bfl} increases above zero. This leads to very flat spectra. As β_{1HT} approaches and eventually exceeds unity, this trend reverses, and σ then rapidly increases with increasing shock obliquity. This is the character of near-luminal and superluminal shocks evinced in the left panel of Fig. 1, precipitated by inexorable convection of particles away downstream of the shock, steepening the distribution dramatically. The only way to ameliorate this rapid decline in the acceleration efficiency is to reduce λ/r_g to values below around 10. Physically, this is tantamount to increasing the hydromagnetic turbulence to high levels that force the particle diffusion to approach isotropy. Then, transport of charges across the mean field becomes significant on gyration timescales, and they can be retained near the shock for sufficient times to accelerate and generate suitably flat distribution functions. Such low values of λ/r_g render the field direction immaterial, and the shock behaves much like a parallel, subluminal shock in terms of its diffusive character. Then, σ is only weakly dependent on Θ_{Bfl} , the second key property illustrated in the right panel.

The origin of the extremely flat distributions with $\sigma \sim 1$ is in the coherent effect of *shock drift acceleration* at the shock discontinuity. This phenomenon has been widely understood in non-relativistic shocks, and is due to the energy gain of charges when they repeatedly encounter $\mathbf{u} \times \mathbf{B}$ electric fields (in frames other than the HT frame) in gyrations straddling the shock discontinuity. The energy gain rate then scales as the gyrofrequency c/r_g , i.e. is proportional to the particle's energy/momentum, so that the equilibrium distribution realized in pure shock drift acceleration is $dN/dp \propto p^{-1}$ [18]. Reducing λ/r_g and thereby introducing extremely modest amounts of cross-field diffusion disrupts this coherence, removes particles from the shock layer, and steepens the spectrum. It is noted in passing that the choice of the somewhat large (for $\beta_{1x} = 0.5$) compression ratio $r = 4$ was to afford direct comparison with the semi-analytic convection-diffusion equation results of Kirk & Heavens [4], which physically correspond to $\lambda/r_g \gg 1$ cases with minimal cross field diffusion. The differences between our simulation indices in this limit and those of [4] arise because the adiabatic approximation employed in [4] to describe shock crossings does not take into account the gyration trajectories of charges in the shock layer. These subtleties are discussed further in [18].

CONSTRAINTS ON ACCELERATION THEORY FROM GRB OBSERVATIONS

Gleaning meaningful insights into the connection between acceleration theory and prompt burst signals hinges upon two aspects: the high energy spectral index α_h ($= -\beta$ for Band model [24] index β), when the differential spectrum is $dn/dE_\gamma \propto E_\gamma^{-\alpha_h}$, and generating burst spectral shape at and below the ν - F_ν peak. These will be considered in turn.

The α_h High-Energy Spectral Index

The high-energy photon spectral indices α_h for the CGRO EGRET and Comptel bursts are tabulated in [25]. One of these EGRET detections, GRB 930131, had an index $\alpha_h \approx 2$, which corresponds to the indication in both panels of Fig. 1 if a synchrotron or inverse Compton cooling model is adopted. This is on the flat end of the EGRET α_h index distribution [26], for which a handful of sources evinced photon differential spectrum indices scattered in the range $2 \lesssim \alpha_h \lesssim 3.7$ (though note that EGRET spark chamber detections were concentrated in the index range $\alpha_h \lesssim 2.8$ [25]). The CGRO BATSE α_h index distribution [27] is similarly broad, but with $1.5 \lesssim \alpha_h \lesssim 3.5$ and far greater statistics. The recent *Fermi* detection of GRB 08016C in both the GBM and LAT instruments offered a high energy index of $\alpha_h \sim 2.2$ in its most luminous epoch, and a steeper spectrum at other times [28]. Accordingly, shock acceleration models must accommodate a radiation spectral index in the range $2 \lesssim \alpha_h \lesssim 4$ in order to be viable.

The phase space for achievability of this depends on the radiation mechanism, and also upon whether or not cooling is invoked. The most popular model scenario for the production of the prompt GRB signal is quasi-isotropic electron synchrotron emission [2, 3]. In this case, as with inverse Compton scattering, the photon differential spectral index is given by $\alpha_h = (\sigma + 1)/2$ above the ν - F_ν peak, if cooling is not efficient, and $\alpha_h = (\sigma + 2)/2$ if the particles are continuously cooled in a large volume before being re-injected into an acceleration process, for which the particle distribution index is steepened by unity. From the Figure, it is evident that this is readily achievable for GRB 930131 for quasi-parallel shocks with perhaps some component of modest angle scattering, or for moderately oblique shocks

as long as $\lambda/r_g \lesssim 3 - 10$. The EGRET GRB index range $2 \lesssim \alpha_h \lesssim 3.7$ then corresponds to diffusive acceleration with $2 \lesssim \sigma \lesssim 5.4$ in the presence of cooling, and $3 \lesssim \sigma \lesssim 6.4$ otherwise. In either case, subluminal shocks, either quasi-parallel ($\Theta_{\text{Bfl}} \lesssim 20^\circ$) or moderately oblique ($20^\circ \lesssim \Theta_{\text{Bfl}} \lesssim 60^\circ$) are required to explain flatter GRB spectra as in GRB 910503, GRB 930131, GRB 950425 or GRB 080916C. For bursts with somewhat larger α_h indices, superluminal shocks can be viable, but only if the scattering is strong, i.e. $\lambda/r_g \lesssim 3 - 10$. Otherwise, convection away from the shock dominates the acceleration, and the electron distribution becomes too steep. For the less popular uncooled hadronic models, the photon and particle indices trace each other, i.e. $\alpha_h = \sigma$, and a similar conclusion that the environment is restricted to subluminal or modestly superluminal oblique shocks is derived. Note that while Lorentz transformations of circumburst fields of arbitrary orientation render ultra-relativistic external GRB shocks quasi-perpendicular ($\Theta_{\text{Bfl}} \approx 90^\circ$), moderate field obliquities are often attained in mildly-relativistic internal shocks.

Discriminating between the σ constraints in the presence or absence of synchrotron cooling mandates a brief discussion of the balance between acceleration and cooling. Diffusive shock acceleration is usually dominated by gyroresonant interactions between charges and hydromagnetic turbulence [29]. If this is the case, then for a charge of Lorentz factor γ , the acceleration rate essentially scales as γ times the particle's gyrofrequency, implying $d\gamma/dt \propto \gamma^0$. In contrast, synchrotron and inverse Compton cooling rates yield $d\gamma/dt \propto -\gamma^2$. Accordingly, simultaneous and co-spatial acceleration and synchrotron cooling yield a power-law distribution with the "raw" acceleration index σ up to a maximum energy where cooling begins to dominate, and generates an exponential turnover. This is the widely considered scenario for X-ray/TeV supernova remnant studies. For external GRB shocks spawning afterglow signals, there is plenty of time for accelerated charges to diffuse away from the shock and subsequently cool, so that the cumulative effect is emission from a cooling-steepened injected power-law. The situation is very different for internal shocks. The acceleration must persist up to the maximum energy seen in the observations, for example 1 GeV in GRB 930131 and 13 GeV in GRB 080916C, and on a timescale Δt commensurate with the variability at these energies, i.e., $\Delta t \lesssim 1$ sec or much less. Cooling breaks, by an index of $\Delta\alpha_h = 1/2$, are not observed above 1 MeV in burst emission, so if the spectra spanning 1 MeV – 10 GeV correspond to a cooling-dominated contribution, the acceleration must operate in short, impulsive periods, followed by long cooling epochs that permit the electrons to decline in momentum by a factor of 10^2 or so. Accordingly, the cooling epochs should possess durations of around 4 orders of magnitude longer than the impulsive acceleration epochs. It is not clear that the superposition of a host of these presumably pseudo-FRED-like profiles can mimic typical burst time histories while maintaining the time-averaged spectral behavior.

Constraints from the ν - F_ν Peak

An additional requirement for the success of an acceleration model is that when convolved with a radiation process such as synchrotron radiation, it can generate the shape of the GRB spectrum around and below the ν - F_ν peak. This was the focus of the investigation by Baring & Braby [14]. Early work on broad-band spectral fitting of bursts was provided by Tavani [30], who obtained impressive fits to time-integrated spectra of several bright CGRO BATSE bursts using a phenomenological electron distribution and the synchrotron emission mechanism. While this succeeded in this limited sample, providing a driver for the popularity of the synchrotron GRB emission model, there are difficulties with fitting low energy (i.e. $\lesssim 100$ keV) spectra in about 1/3 of bursts [31]. Employing perspectives based on acceleration theory, this investigative effort was extended and refined by [14], who pursued a program of spectral fitting of GRB emission using a linear combination of thermal and non-thermal electron populations. These fits demanded that the preponderance of electrons that are responsible for the prompt emission reside in an intrinsically non-thermal population. Such a constraint, dictated by the narrowness of the ν - F_ν peak, is commensurate with electron distributions frequently presumed in GRB spectral models, i.e. truncated power-laws. Yet, this requirement strongly contrasts particle distributions obtained from acceleration simulations, exemplified by those depicted in Fig. 1, and further illustrated in numerous papers [6, 7, 9, 16, 17]. Moreover, particle-in-cell (PIC) plasma simulations [10–12] generally exhibit largely Maxwellian distributions, and in the isolated recent suggestion [13] of a non-thermal tail generated by diffusive transport, the thermal population strongly dominates the high-energy tail.

The consequence is obviously a potential conflict for acceleration models, since the non-thermal electrons are almost always drawn directly from a thermal gas. This does not necessarily mean that acceleration at relativistic shocks is not precipitating the prompt emission. It is possible that somehow, relativistic shocks can suppress thermalization of electrons, though such a conjecture presently has no simulational evidence to support it. Or, radiative efficiencies might become significant only at highly superthermal energies: a convenient resolution to this dilemma is that strong radiative self-absorption could be acting, in which case ν - F_ν peaks (and therefore BATSE and *Fermi* GBM spectral probes) are

not actually sampling thermal electrons. It is also possible that other mechanisms such as pitch-angle synchrotron, or jitter radiation may prove more desirable. A cautionary note is that this complication for the interpretation is predicated upon spectra integrated over the burst duration, which can differ significantly from those obtained in temporal sub-intervals (e.g. see [28]). Notwithstanding, cumulative spectra provide a global indication of a narrowness of the MeV spectral break, and this must be a characteristic of at least the most luminous portions of the burst time history. We note also that [14] concluded that the synchrotron self-Compton process was unlikely to be able to generate the MeV band emission in prominent EGRET bursts because of its intrinsic spectral breadth, even with extremely narrow electron distribution functions. Only a self-absorption in the synchrotron seed spectrum can aid its viability.

CONCLUSION

This paper explores the connection between diffusive shock acceleration theory and prompt emission in bursts. Simulation results presented clearly highlight the non-universality of the index of energetic, non-thermal electrons and ions, spawned by the variety of shock obliquities and the character of hydromagnetic turbulence in their environs. This non-universality poses no problem for modeling GRB high-energy power-law indices, though observations generally constrain the parameter space to subluminal or highly-turbulent superluminal shocks near the Bohm diffusion limit. Also, demanding a connection between the thermal electron population and the GRB ν - F_ν peak gives rise to an inconsistency in that acceleration simulations predict a dominance of the thermal population, whereas the radiation models demand that the contributing particles are intrinsically non-thermal. Escape clauses include invoking radiative self absorption, or perhaps relinquishing preferred emission mechanisms, i.e., synchrotron or inverse Compton radiation. The prospect of a number of platinum standard, broad-band GRB detections by *Fermi* that permit time-dependent spectroscopy should hone our understanding of the connection between shock acceleration and prompt emission.

Acknowledgments: this research was supported in part by NASA grant NNG05GD42G and NSF grant 0758158.

REFERENCES

1. Rees, M. J. & Mészáros, P. 1992, *M.N.R.A.S.*, **258**, 41P.
2. Piran, T. 1999, *Phys. Rep.*, **314**, 575.
3. Mészáros, P. 2002, *Ann. Rev. Astron. Astr.*, **40**, 137.
4. Kirk, J. G. & Heavens, A. F. 1989, *M.N.R.A.S.*, **239**, 995.
5. Kirk, J. G., Guthmann, A. W., Gallant, Y. A., Achterberg, A. 2000, *ApJ*, **542**, 235.
6. Ellison, D. C., Jones, F. C. & Reynolds, S. P. 1990, *ApJ*, **360**, 702.
7. Ellison, D. C. & Double, G. P. 2004, *Astroparticle Phys.*, **22**, 323.
8. Niemiec, J., & Ostrowski, M. 2004, *ApJ*, **610**, 851.
9. Stecker, F. W., Baring, M. G. & Summerlin, E. J. 2007, *ApJ*, **667**, L29.
10. Hoshino, M., Arons, J., Gallant, Y. A. & Langdon, A. B. 1992 *ApJ*, **390**, 454.
11. Nishikawa, K.-I., et al. 2005, *ApJ*, **622**, 927.
12. Medvedev, M. V., et al. 2005, *ApJ*, **618**, L75.
13. Spitkovsky, A. 2008, *ApJ*, **682**, L5.
14. Baring, M. G. & Braby, M. L. 2004, *ApJ*, **613**, 460.
15. Jones, F. C. & Ellison, D. C. 1991, *Space Sci. Rev.*, **58**, 259.
16. Ellison, D. C., Baring, M. G. & Jones, F. C. 1995, *ApJ*, **453**, 873.
17. Summerlin, E. J. & Baring, M. G. 2006, *Adv. Space Res.*, **38(7)**, 1281.
18. Baring, M. G. & Summerlin, E. J. 2009, *Adv. Space Res.*, in preparation.
19. Bell, A. R. 1978, *M.N.R.A.S.* **182**, 147.
20. Giacalone, J., Burgess, D., & Schwartz, S. J. 1992, in *ESA, Study of the Solar-Terrestrial System*, 65.
21. Forman, M. A., Jokipii, J. R. & Owens, A. J. 1974, *ApJ*, **192**, 535.
22. Baring, M. G. 2004, *Nucl. Phys. B*, **136C**, 198.
23. de Hoffman, F. & Teller, E. 1950, *Phys. Rev. D*, **80**, 692.
24. Band, D. L., et al. 1993, *ApJ*, **413**, 281.
25. Baring, M. G. & 2006, *ApJ*, **650**, 1004.
26. Dingus, B. L. 1995, *Astr. Space Sci.*, **231**, 187.
27. Preece, R. D., et al. 2000, *ApJ Supp.*, **126**, 19.
28. Abdo, A. A., et al. (for the *Fermi* Collaboration) 2009, *Science*, submitted.
29. Drury, L. O'C. 1983, *Rep. Prog. Phys.*, **46**, 973.
30. Tavani, M. 1996, *Phys. Rev. Lett.*, **76**, 3478.
31. Preece, R. D., Briggs, M. S., Malozzi, R. S., et al. 1998, *ApJ*, **506**, L23.